Recommended by Chief Classified Open Pub. 2 June 69 OASD Rl. Dod

AD

AD 710821

1852-9-F(I)

RADIOMETRIC MEASUREMENTS OF MUZZLE FLASH

Final Report

Volume I: Program Design and Procedure

BY

A. J. LaROCCA

G. H. LINDQUIST

J. P. LIVISAY

C. J. GREEN

Sponsored by the Advanced Research Projects Agency, Department of Defense, ARPA Order No. 859-7, and monitored by the U. S. Army Missile Command under Contract DAA[illegible]01-C-1475.

68

APRIL 1969

Distribution Statement Unlimited

This document is subject to special export controls and each transmittal to foreign governments or foreign nationals may be made only with prior approval of Assistant Chief of Staff for Intelligence, ATTN: ACSI-[illegible], Washington, D. C.

INFRARED AND OPTICS LABORATORY

Willow Run Laboratories

INSTITUTE OF SCIENCE AND TECHNOLOGY

THE UNIVERSITY OF MICHIGAN

Ann Arbor, Michigan

AUG 27 1970

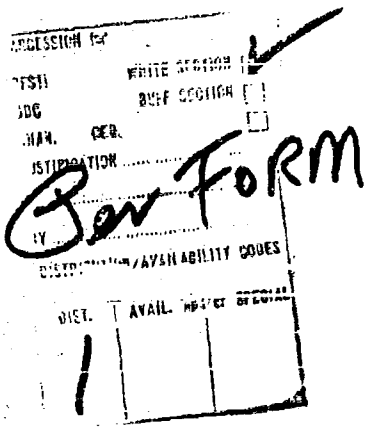

FORM 50

NOTICES

Sponsorship. The work reported herein was conducted by the Willow Run Laboratories of the Institute of Science and Technology for the Advanced Research Projects Agency, Department of Defense, and was monitored by the U. S. Army Missile Command under Contract No. DAAH01-68-C-1475. Contracts and grants to The University of Michigan for the support of sponsored research are administered through the Office of the Vice President for Research.

Disclaimers. The findings in this report are not to be construed as an official Department of the Army position, unless so designated by other authorized documents.

The citation of trade names and names of manufacturers in this report is not to be construed as official Government indorsement or approval of commercial products or services referenced herein.

Disposition. Destroy this report when it is no longer needed. Do not return it to the originator.

1652-9-F(ii)

RADIOMETRIC MEASUREMENTS OF MUZZLE FLASH

Final Report

Volume I: Program Design and Procedure

BY

A. J. LaROCCA

G. H. LINDQUIST

J. P. LIVISAY

C. J. GREEN

Sponsored by the Advanced Research Projects Agency, Department of Defense, ARPA Order No. 859-7, and monitored by the U. S. Army Missile Command under Contract DAAH01-C-1475.

APRIL 1969

Distribution Statement Unlimited

This document is subject to special export controls and each transmittal to foreign governments or foreign nationals may be made only with prior approval of Assistant Chief of Staff for Intelligence, ATTN: ACSI-FE, Washington, D.C.

INFRARED AND OPTICS LABORATORY

Willow Run Laboratories

INSTITUTE OF SCIENCE AND TECHNOLOGY

THE UNIVERSITY OF MICHIGAN

Ann Arbor, Michigan

This document has been approved for public release and sale; its distribution is unlimited.

FOREWORD

Because the results of this program can easily be divided into two sections, one Unclassified and the other Confidential, we have decided to publish this final report in two volumes. Volume I (Unclassified) includes discussion of the design of the measurement program and description of the instruments used, their calibration, and the procedure used in obtaining and reducing the data. Volume II (Confidential) presents a discussion and analysis of the results obtained. Data from the following weapon types are described: 175-mm gun, 155-mm howitzer, 105-mm howitzer, 90-mm gun, 75-mm gun, 40-mm gun, 4.2-in. mortar, and 81-mm mortar. Some 60-mm mortars with zero charge were also observed but produced signal levels which were too low to yield good results.

ABSTRACT

Volume I begins with a description of the design of a program to measure the radiation from weapon muzzle flash in the spectral region from 0.8 to 5 μm. Instruments designed to measure the spectral radiant intensity and spectral radiance of these phenomena in narrow spectral bands are described. A discussion of the calibration techniques used to quantify accurately and precisely the results from the instruments is also included. The results of the measurements obtained are presented in Volume II.

CONTENTS

Foreword iii
Abstract v
List of Figures viii
1. Introduction 1
2. Program Design 2
3. Description of the Radiometers 4
   3.1. Wide Field of View 4
   3.2. Narrow Field of View 4
   3.3. Electronics 5
4. Calibration 7
   4.1. Field-of-View Contours 7
   4.2. Filter Characteristics 8
   4.3. Responsivity 13
   4.4. Calibration Lamps 21
   4.5. Atmospheric Transmittance 27
   4.6. Temporal Response 28
5. Measurement Procedure 32
6. Data Reduction 36
7. Summary 37
References 39
Distribution List 40

FIGURES

1. Diagram of the WFOV Radiometer 5
2. Transmittance of the Irtran 2 Lens 6
3. Diagram of the NFOV Radiometer 6
4. Plot of Field of View for Radiometer #1 with a 2.2-μm Filter 9
5. Plot of Field of View for Radiometer #3 with a 2.2-μm Filter 9
6. Plot of Field of View for Radiometer #4 with a 2.2-μm Filter 9
7. Plot of Field of View for Radiometer #6 10
8. Plot of Field of View for Radiometer #7 10
9. Plot of Field of View for Radiometer #8 10
10. Filter Characteristics 11
11. Signal Voltage vs. Spectral Radiance with Four Filters for Radiometer #6 16
12. Signal Voltage vs. Spectral Radiance with Four Other Filters for Radiometer #6 16
13. Signal Voltage vs. Radiance in $\Delta\lambda$ for Radiometer #6 17
14. Signal Voltage vs. Radiance in $\Delta\lambda$ for Radiometer #7 17
15. Signal Voltage vs. Spectral Radiance with Three Filters for Radiometer #7 18
16. Signal Voltage vs. Radiance in $\Delta\lambda$ for Radiometer #7 18
17. Signal Voltage vs. Spectral Radiance with Three Filters for Radiometer #8 19
18. Signal Voltage vs. Spectral Radiance with Two Filters for Radiometer #8 19
19. Signal Voltage vs. Spectral Irradiance with Three Filters for Radiometer #1 23
20. Signal Voltage vs. Spectral Irradiance with Three Filters for Radiometer #1 23
21. Signal Voltage vs. Spectral Irradiance with Four Filters for Radiometer #2 24
22. Signal Voltage vs. Spectral Irradiance with Four Filters for Radiometer #3 24
23. Signal Voltage vs. Irradiance in $\Delta\lambda$ for Radiometer #3 25
24. Signal Voltage vs. Spectral Irradiance with Three Filters for Radiometer #3 25
25. Signal Voltage vs. Spectral Irradiance with Four Filters for Radiometer #4 26
26. Signal Voltage vs. Irradiance in $\Delta\lambda$ for Radiometer #4 26

27. Diagram of Detector Preamplifier 30
28. Diagram of Pulse Response 33
29. Photograph of Radiometers Set Up to Observe 81-mm Mortars, 8/27/68 34
30. Photographs of Radiometers Set Up to Observe the 75-mm Gun 35
31. Relationship Between Field of View of the NFOV Radiometers and the Gun Muzzle 35

RADIOMETRIC MEASUREMENTS OF MUZZLE FLASH
Final Report
Volume I: Program Design and Procedure

1
INTRODUCTION

The need for determining automatically the location of hostile artillery and heavy infantry pieces is obvious when one considers the complex interaction of threat and environment. Without a sound knowledge of the radiative characteristics of both, the task of designing a system to perform the location function is laden with uncertainties. The purpose of the program described in this report was to increase our knowledge of the radiative characteristics of certain threats, specifically those weapons, guns, howitzers and mortars, ranging in size from 40 mm to 175 mm. The latest substantial information known to exist regarding the radiation from muzzle flash is contained in a group of reports by the Franklin Institute (refs. 1 and 2 for example) which resulted in an Army manual [3]. The spectral data reported in reference 3 are probably useful out to about 2 μm in a relative sense, but the nature of the calibration makes it impossible to obtain radiant intensity values from those results. Further, uncertainty in the spatial extent of the flash coupled with some uncertainty in the meaning of the units of the reported data puts the results in doubt even as determinations of radiance.

Underlying the rationale for the choice of a measurement program was a twofold intent: (1) to gather sufficient data hopefully, to model the infrared radiation from different guns, and (2) to obtain basic information on this radiation to understand the radiative characteristics of muzzle flash as related to the physical and thermodynamical properties of the plume. Although these objectives are not incompatible, the design of an experimental program depends to some extent on what is emphasized.

There is still a third factor, essential in determining the kind of data needed, which is identified here as the systems input. If we are eventually to use the data in design concepts for systems employed in the location of weapons, we are less interested in the basic knowledge of radiative characteristics than in the specific characteristics of enemy weapons. On the other hand, the weapons available for study are those in the U. S. arsenal, and these are somewhat inappropriate as specific entities for systems focalization. Therefore, we attempted to combine the two original objectives as much as possible in a limited experimental program to yield results useful also in a study of systems design concepts.

In order that the experimental results contribute to a basic understanding of the phenomenon of muzzle flash, as well as yield a useful group of models, the program was designed to obtain as many spectral and spatial data as was feasible. The rapid growth and decay in size and intensity of the flash makes it impossible without very sophisticated and expensive equipment to analyze it in very great detail. The spatial information was limited to that obtained by incorporating two fields of view, one large enough to observe the entire plume at any time and hence measure its radiant intensity and one small enough to observe the radiance of only a small portion of the plume near the muzzle exit. Both fields of view were fixed by the focal length of the optics and the size of the field stop in the radiometers used.

Spectral information was obtained by using narrow-band filters in the radiometers. The filters were interchangeable and could be used in any one of the six radiometers employed in a given measurement. Three radiometers had wide fields of view (WFOV) and the other three narrow fields of view (NFOV). The choice of separate, filtered radiometers was made to avert the cost and complication of a dispersing instrument designed to include the difficult spectral interval between 2.5 and 5.5 μm for which complex detectors would have to be used. Complications were inherent in the brute-force handling of a large number of instruments and in an experimental design which had to adapt to an uncertain firing schedule.

2
PROGRAM DESIGN

The program was designed in an effort to obtain time-resolved, spectrally resolved measurements of the radiant intensity of the total flash from the muzzle and of the radiance near the muzzle exit. Temporal fidelity of the radiometers had to be sufficient for resolution of pulses with durations of the order of a few milliseconds and rise times of a fraction of a millisecond. Spectral resolution was ascertained by the expected spectral structure of the radiation, the bandwidths with which filters can be easily made, the expected amoun of power in a narrow spectral region, and the total number of measurements which ultimately have to be made to obtain the required data.

Because potentially a very large quantity of data could be derived from the experimental program, the modus operandi was a compromise between experimental technique and availability of targets. The most sophisticated (and, incidentally, ideal) approach to the measurement of muzzle flash is to use an instrument which partitions the spectrum of the flash at any instant, without interfering with the instrument's ability to respond faithfully to temporal changes of radiant intensity in any spectral region coming from any chosen part of the plume. This paragon of all measuring instruments does not exist simply because the information inherent in this demand exceeds the current infrared state of the art.

However, our basic knowledge of the generalized characteristics of gaseous radiation partially precludes the need for such an instrument. It is necessary only to measure in those spectral regions which one would expect to use in a practical system. On the other hand, since we are also interested in a complete description of muzzle flash, we wanted to sample the entire spectral region of interest. Since practicality limits us to spectral resolutions of the order of 0.1 μm, we chose to sample the spectrum at 0.2-μm intervals with filters of a nominal bandwidth of 0.1 μm. A rapid-scan spectrometer would have been useful to obtain the spectrum with one or two filtered radiometers providing the calibration in a few chosen spectral regions. Although instruments exist which would provide the data needed for this program, they exist only in designs for laboratory use and are very expensive to build.

From the known limitations on measurement imposed by attenuation of radiation by the atmosphere, it was possible to limit the number of filters used in the radiometers still further. Furthermore, by examination of typical spectra of combustion exhausts containing H_2O vapor and carbon products, one can identify those regions in the spectrum at which the strongest radiation is likely to occur for relatively short-distance measurements. Thus, we find that we should seek those regions outside of complete absorption by the atmosphere, yet within the wings of atmospheric absorption where the emitter is still strong enough to produce a sizable signal. The actual regions chosen are shown in section 3.

It will be noted that a wide-band filter was added in the region between 2 and 2.5 μm where the high signal might conceivably prove useful for detection purposes. An integration of spectral power in this interval might provide useful information for systems designers. A wide-band filter was also used between 3.4 and 4 μm, where the power level was low enough to require this integration of the spectral power. In addition, it should be pointed out that because stock filters were used (being much cheaper than custom-made filters) it was not always possible to achieve center wavelengths precisely where the peak of radiation was expected. On the other hand, because spectral peaks in the radiation from such sources shift radically within a range of several 1/100ths of a micrometer with changes of distance (and concomitant changes in atmospheric absorptance) between source and receiver, the urgency to pinpoint the center wavelength was not overwhelming.

The spatial resolution of the radiometers was a compromise chiefly between the sizes of detectors used and the amount of power emitted in the flash. The basic optical systems for the radiometers existed before this program was initiated. It was necessary, therefore, to prescribe detector sizes in accordance with the fields of view desired. For the purpose of maintaining interchangeability, the detectors obtained were all the same size, approximately 2.5-mm square. Subsequently, however, we were unable to take advantage of interchanging detectors, and the resulting systems incorporating the two different fields of view were entirely independent.

We did not attempt a truly randomized design of the experiment. Rather we tried to get an even distribution of measurements among the different filter regions. Several factors helped prevent a statistical experimental design; the two most important were the absence of certain filters during part of the program and the unavailability of certain weapons for observation at prescribed times. The result was that a large number of measurements were obtained, but the distribution among the different spectral regions was not as uniform as was desired. The failure of the long wavelength detector resulted in a complete lack of data in the spectral region from 8 to 13 μm.

3
DESCRIPTION OF THE RADIOMETERS

3.1. WIDE FIELD OF VIEW

Figure 1 is a schematic drawing of the WFOV radiometer used to obtain radiant intensity measurements of the muzzle flash. It consists of an Irtran 2 lens for collecting and focussing the radiation on a detector which transduces the radiation to a voltage which is amplified and recorded on a tape recorder. The transmitting characteristic of the Irtran 2 lens is shown in figure 2. Note that for wavelengths below 1 μm and above 14 μm the Irtran 2 lens is relatively non-transmitting. Thus, data collected between 0.8 and 1.5 μm is probably subject to more uncertainty than the rest.

Since this radiometer was adapted from an earlier design, it incorporated an end-looking detector. To keep the detector vertical, it was necessary to provide a 45° mirror to reflect upward the horizontally approaching radiation. One of several different filters was interposed between the incoming radiation and the lens to provide the spectral selectivity necessary.

The detector (InAs for the spectral region 0.8 to 3 μm, InSb for 3 to 5.5 μm), was mounted in a ring which could be moved up and down on a rack and pinion for relatively easy focussing of radiation on the detector.

3.2. NARROW FIELD OF VIEW

Figure 3 is a schematic representation of the radiometer used to obtain radiance values of the muzzle flash. The speed of the optical system combined with the size and shape of a circular aperture (1 mm in diameter) in front of the detector yields a circular field of view approximately 2.5 mrad in diameter. Thus, the area subtended at the gun for a distance of 100 ft is a circle about 3 in. in diameter. This size is correspondingly larger for the greater distances incorporated in measurements on the larger guns.

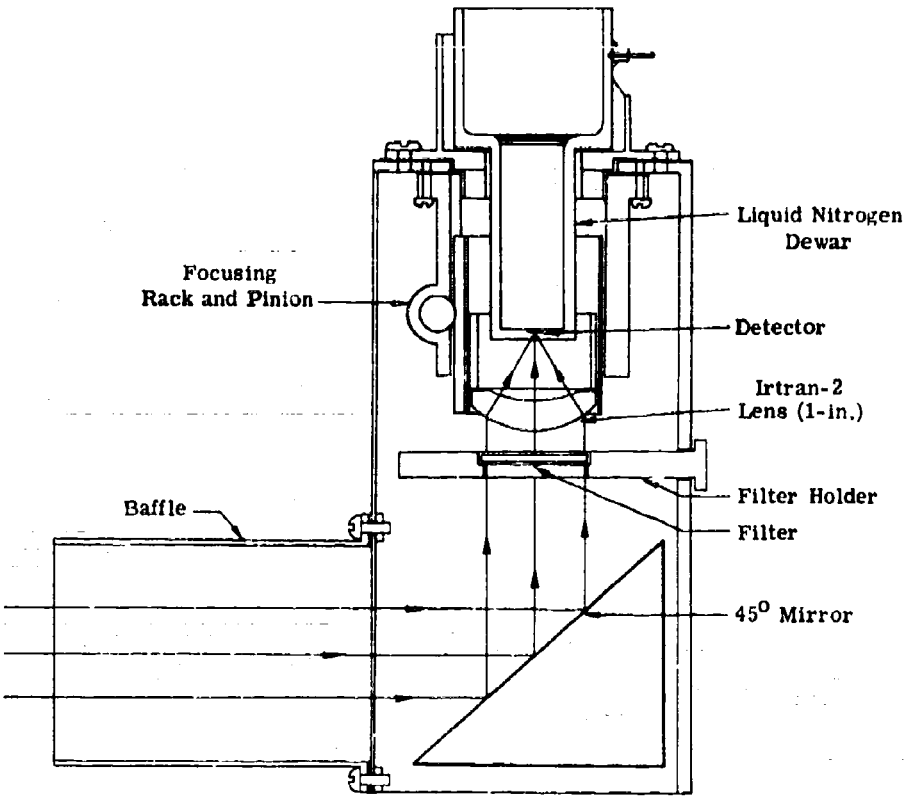

FIGURE 1. DIAGRAM OF THE WFOV RADIOMETER

The optical system is Cassegrainian with a primary diameter of about 6 in. and a secondary diameter of 3 in. A side-looking detector rides on a rack and pinion for easy focussing. The filter, in a specially designed holder, is interposed between the detector and the beam of energy coming through the hole in the primary mirror. As with the NFOV radiometers, the detectors used were InAs for the short wavelength region to about 3 μm, InSb for the spectral region from 3 to 5.5 μm, and Hg:Cd:Te intended for use in the 8- to 13-μm region. The filters were interchangeable between the two types (WFOV and NFOV) of radiometers.

3.3. ELECTRONICS

Each of the WFOV and NFOV radiometers used identical electronics. The photocurrent from the detector was amplified by a self-biasing current-to-voltage preamplifier which in turn drove a 500-ft coaxial cable connected to a postamplifier mounted in the equipment van.

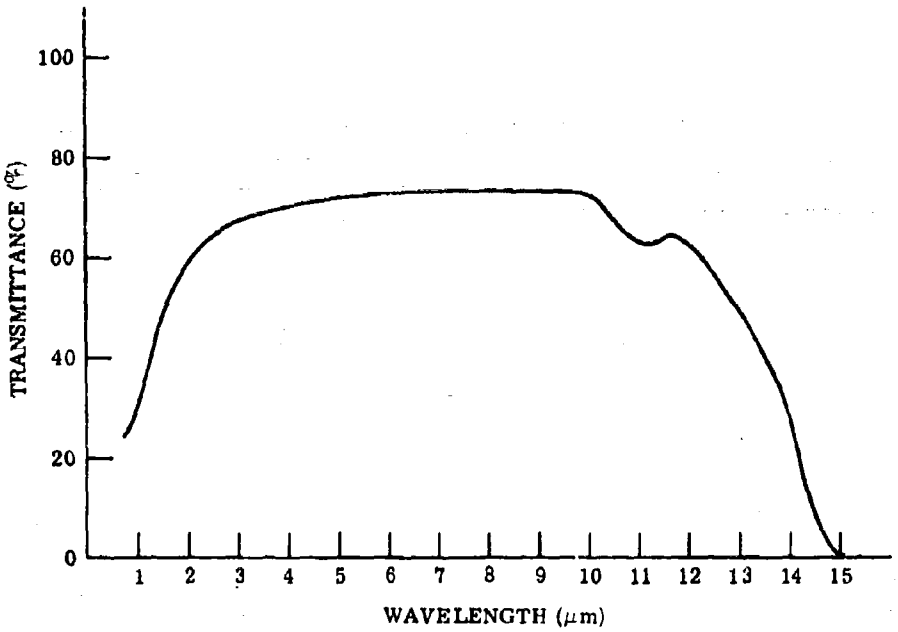

FIGURE 2. TRANSMITTANCE OF THE IRTRAN 2 LENS

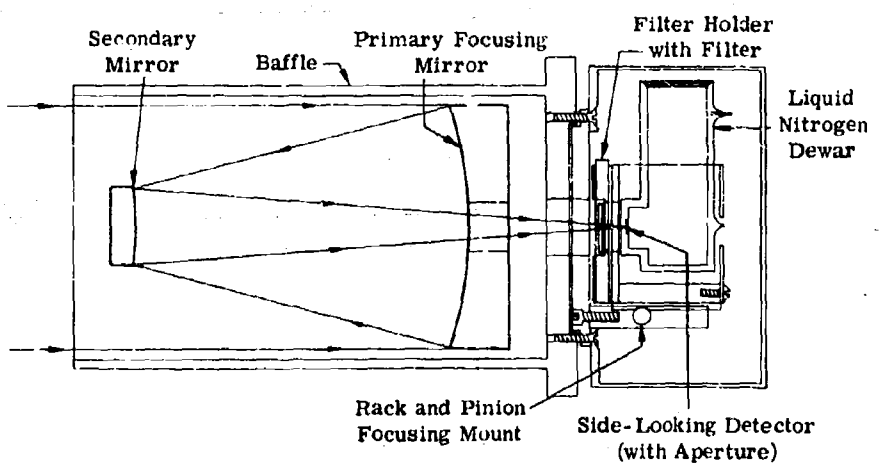

FIGURE 3. DIAGRAM OF THE NFOV RADIOMETER

The postamplifiers had been built on another project from discrete component operational amplifiers. They had known, stable gains through the use of precision metal film resistors as feedback elements. Five values of gain were switch selectable. The outputs of the postamplifiers were fed to the inputs of a 14-channel, 1-in. tape recorder operating at 60 ips. The signals were recorded in the FM/FM mode to preserve the low frequency components of the signal. Periodically, a 2-V, regulated square wave was fed to all inputs of the tape recorder to calibrate the record-reproduce relationship.

4
CALIBRATION

Calibration of the instruments comprises a series of basic measurements which must be carefully performed to yield a base for creating sound, absolute data with a high level of confidence. This is the most important single part of the measurement program.

4.1. FIELD-OF-VIEW CONTOUR

To understand the meaning of the field-of-view contour, consider a simple optical system consisting of a collector and detector (an inaccurate description of the system used in these reported measurements). In an ideal, non-diffraction-limited optical system, the object and image (detector or other field stop) planes are conjugate so that the detector or field stop can be imaged in its conjugate object plane in a perfect representation of itself. For a simple, uniformly responding surface, a representation of the surface sensitivity, as obtained by observations with the radiometer of a point source at the focussed distance, is a constant signal value within the geometrical limits of the image of the detector (or field stop) edge, and zero outside of these limits.

If the detector exhibits non-uniform sensitivity across its surface, then the signal out will not be a constant value as the point source is moved across its image in the plane in which the source is moved. Instead the signal will embody these non-uniformities, and a plot of the signal for different points in the detector image plane will yield contours of constant sensitivity.

The field-of-view contour provides an understanding of the relationship between the spatial character of the radiating source and the spatial character of the optical system and detector which receive the radiation. For the ideal, non-diffraction-limited optical system, the solid angle field of view, ω, would be defined very approximately (for $r >> f$) by the relation

$$\omega = a_d/f^2 = A_d/r^2$$

where a_d is the area of detector or field stop, f is the focal length of the instrument, and A_d is the area of the detector image at its conjugate distance r from the collector optics. However, aberrations in the optics, non-uniformities in the detector, lack of proper focussing, and finite size of the test point source tend to modify the field of view from the ideal to that determined in reality. Field-of-view contours for the WFOV radiometers are shown in figures 4, 5, and 6. Those for the NFOV radiometers are shown in figures 7, 8, and 9.

It will be noted from figures 4 and 6 that the field of view of radiometers #1 and #4 (measured with the 2.2-μm filter in place) are almost what would be calculated geometrically from known optical constants. Thus, the field of view of each of these radiometers is 6° from one side to the other with highly acceptable uniformity. Radiometer #3 shows a slight deviation from the ideal with an unexplained slight contour irregularity at 3 o'clock. All of the WFOV radiometers show sufficient uniformity over a wide enough area that, as long as the radiometer optics was centered on the flash, unambiguous, accurate results should have been obtained. The highly sensitive, uniform portion of the field of view was sufficiently large to encompass the whole of all muzzle flashes except the few exceptionally large ones. By definition then, the WFOV radiometers were in reality capable of measuring the time-varying radiant intensity of the flash.

The fields of view of the NFOV radiometers (figs. 7-9) did not display the desirable sharp, circular contours obtainable from calculation, although radiometer #6 (fig. 7) came fairly close to the ideal. Except for the irregularity and the slow gradient exhibited by radiometers #7 and #8 (figs. 8 and 9), the average diameter of each field of view was approximately 2 mrad, which defined a circle of projected diameter at the gun muzzle of approximately 2.5 in. for every 100-ft distance between radiometer and gun.

Because the NFOV radiometers were calibrated in terms of the source radiance (i.e., with uniform radiation filling the detector), non-uniformities in the field of view would have no adverse effect on determining the radiance of a specific area of the source if the part of the source sampled were uniform. That is, unambiguous results could be obtained. However, if non-uniformity exists in the sampled area, then the convolution of the two non-uniformities (source and field of view) yields results which can be interpreted only with a careful analysis of all the data, including the physical properties of the flash. Furthermore, even with a perfectly uniform and well-defined field of view, the best that can be obtained if the flash is non-uniform is an average value of the radiance.

4.2. FILTER CHARACTERISTICS

For the purpose of limiting the data to the spectral regions of interest, filters are inserted in the radiation beam. Characteristics of the filters used in this program are shown in figure 10.

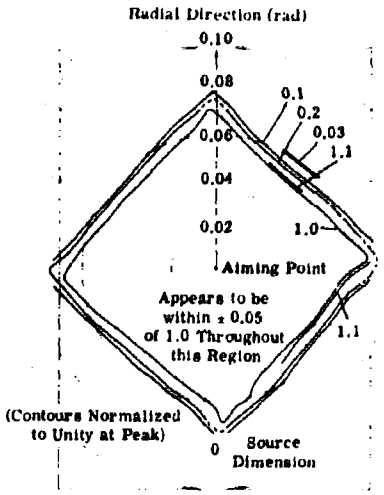

FIGURE 4. PLOT OF FIELD OF VIEW FOR RADIOMETER #1 WITH A 2.2-μm FILTER

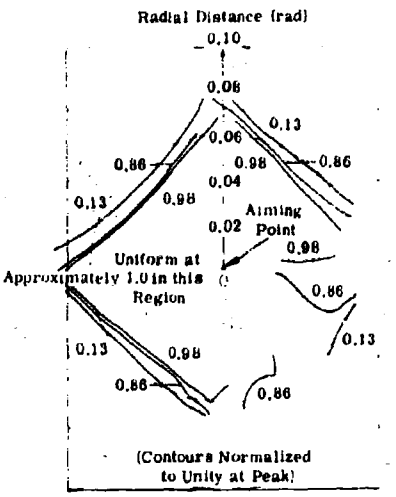

FIGURE 5. PLOT OF FIELD OF VIEW FOR RADIOMETER #3 WITH A 2.2-μm FILTER

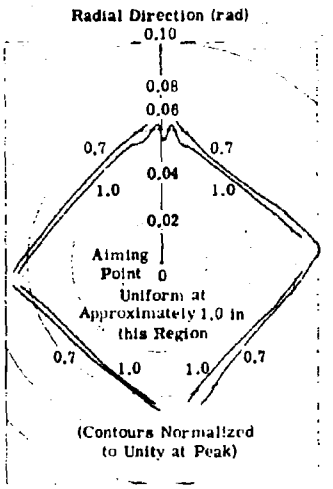

FIGURE 6. PLOT OF FIELD OF VIEW FOR RADIOMETER #4 WITH A 2.2-μm FILTER

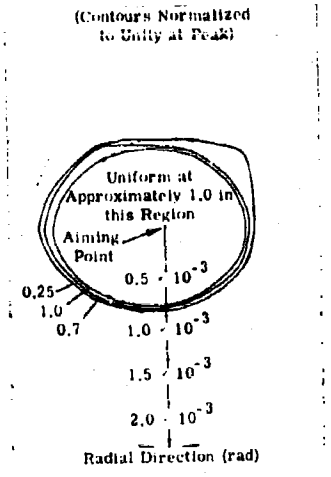

FIGURE 7. PLOT OF FIELD OF VIEW FOR RADIOMETER #6

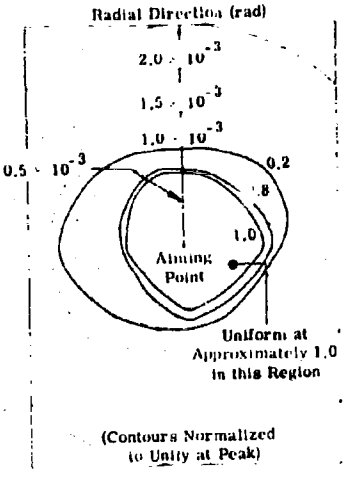

FIGURE 8. PLOT OF FIELD OF VIEW FOR RADIOMETER #7

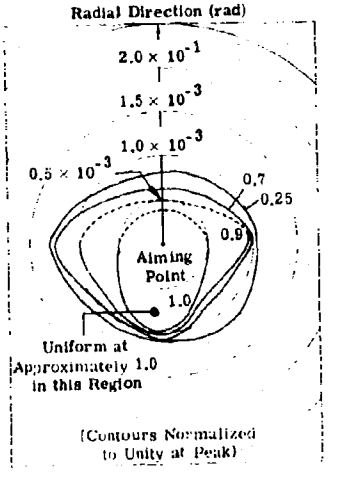

FIGURE 9. PLOT OF FIELD OF VIEW FOR RADIOMETER #8

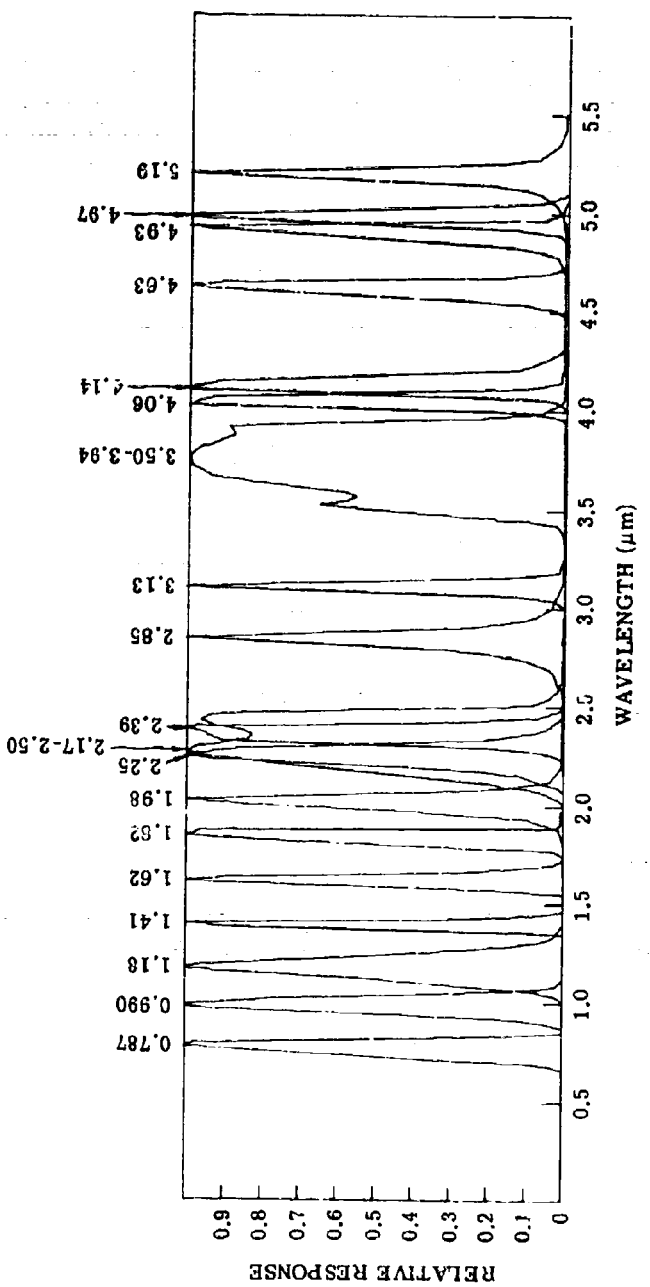

FIGURE 10. FILTER CHARACTERISTICS

All filters are presented on one graph and normalized to unity for comparison of the spectral regions sampled. The actual peak transmittance of the filters is given in table I. As specified in the planning of the program, the center wavelengths of the filters are approximately 0.2 μm apart except in and near the strong atmospheric absorption regions. No measurements were made in the centers of these regions, and attempts were made to sample in the wings of the H_2O and CO_2 atmospheric bands where target radiation managed to leak through. Note also the wide-band filters between 2.17 and 2.50 μm and between 3.50 and 3.94 μm.

The filter centered at 2.85 μm became degraded toward the end of the measurement program, and its characteristics changed slightly; a slight widening of the bandwidth occurred, and a small tail on the long wavelength side developed. Analysis of the data would naturally have to take this into consideration, although the interpretation of a change in observed values would be difficult because of the superposition of two changing entities: the spectral transmittance of the filter and the spectral emittance of the gun flash.

TABLE I. FILTER CHARACTERISTICS

Filter No.	Center λ (μm)	Filter Bandwidth $\Delta\lambda$ (μm)	Peak τ (%)	Average τ (%)
1	0.787	0.091	9.7	
2	0.990	0.096	58.8	
3	1.18	0.050	33.4	
4	1.41	0.133	47.0	
5	1.62	0.067	37.4	
6	1.82	0.076	46.0	
7	1.98	0.093	55.2	
8	2.25	0.123	48.5	
9	NA (wide band)	0.310		67.5
10	2.39	0.100	61.0	
11	2.85	0.106	65.9	
12	3.13	0.064	64.7	
13	NA (wide band)	0.407		80.0
14	4.06	0.077	57.0	
15	4.14	0.070	53.0	
16	4.63	0.090	62.2	
17	4.93	0.094	65.8	
18	4.97	0.073	66.0	
19	5.19	0.087	53.0	

The bandwidths were very near to the specified value of 0.1 μm. The spectral bandwidth is calculated simply from the expression

$$\Delta\lambda = \frac{100}{\tau'_{\text{peak}}} \int_{\lambda_1}^{\lambda_2} \tau'(\lambda)\, d\lambda$$

The filter curves were digitized and the integral easily computed numerically using as λ_1 and λ_2 the points beyond which $\tau'(\lambda)$ is zero. Of all the optical components in the radiometer which can vary spectrally, the filter transmission varies more rapidly with wavelength than any other and so essentially determines the spectral sensitivity of the radiometer.

4.3. RESPONSIVITY

The signal output from a filtered radiometer follows the form of

$$V = \frac{\mathscr{R}}{D^2} \int_0^{\infty} L_\lambda(\lambda) \cdot \alpha \cdot A \cdot \tau(\lambda) \cdot s(\lambda)\, d\lambda$$

where V = signal out of the detector

D = distance in centimeters to the emitting source

$L_\lambda(\lambda)$ = radiance of the (uniform) source

α = area of the source observed by the instrument

A = area of the collecting optics

$\tau_a(\lambda)$ = transmittance of the atmosphere

$s(\lambda)$ = (normalized to unity) dimensionless spectral response of the instrument which, for narrow-band filters, has approximately the shape of the filter transmittance

λ = wavelength in micrometers

The quantity $\mathscr{R}$ is a constant of proportionality called the responsivity, having dimensions of volts per watt in the above equation. Its nomenclature is otherwise determined by the quantity being measured as shown below.

4.3.1. NARROW-FIELD-OF-VIEW RADIOMETERS. In calibrating the NFOV radiometer, we are interested in the radiance of the source. We note that the quantity $\alpha/D^2 = \omega$, the field of view of the radiometer, is a constant of the system. By combining this with the other constants A and $\mathscr{R}$, we end up with $\mathscr{R}' = \mathscr{R}A\omega$, the radiance responsivity of the system, which is the signal voltage (or some other observable) out of the system related to the amount of radiance measured in the integrated spectral region. Thus, we may write

$$V = \mathscr{R}' \int_0^{\infty} L_\lambda(\lambda) \cdot \tau_a(\lambda) \cdot s(\lambda)\, d\lambda$$

We realize, of course, that for a distant source the instrument response is proportional to $L_\lambda(\lambda) \cdot \tau_a(\lambda) = L'_\lambda(\lambda)$, the apparent spectral radiance and not the true radiance. In order to obtain the true radiance from the calibration data, the atmospheric transmittance must be treated.

In the calibration, however, conditions can be met such that $\tau_a(\lambda) \sim 1$, so it becomes necessary only to supply a source of known radiance, which is done by the use of a well-controlled blackbody. For the wide-band filters at 2.17-2.50 μm and 3.50-3.94 μm (where the total integrated radiance over the spectral band was considered instead of the spectral radiance, i.e., per micrometer) the calibration constant, or radiance responsivity, is calculated from

$$\mathscr{R}' = \frac{V}{\int_{\lambda_1}^{\lambda_2} L_{\lambda,BB}(\lambda) \cdot s(\lambda)\, d\lambda}$$

The subscript BB designates that $L_\lambda(\lambda)$ is the blackbody spectral radiance. The dimensions here would be $V/(W\text{-}cm^{-2}\text{-}sr^{-1})$ in the spectral region $\Delta\lambda$, the bandwidth of the filter. The region of integration, λ_1 to λ_2, is the region of sensible transmittance of the filter. In practice, $\mathscr{R}'$ is obtained by plotting a curve of the preamplifier output voltage versus radiance input; that is, the value of the integral in the denominator of the equation.

For the narrow-band filters the value $\mathscr{R}'$ is modified slightly to $\mathscr{R}'_1$ as shown below

$$\mathscr{R}'_1 = \frac{V}{\frac{1}{\Delta\lambda}\int_{\lambda_1}^{\lambda_2} L_{\lambda,BB}(\lambda) \cdot s(\lambda)\, d\lambda}$$

where

$$\Delta\lambda = \int_{\lambda_1}^{\lambda_2} s(\lambda)\, d\lambda$$

Note that in comparison with the previous definition of $\Delta\lambda$, $s(\lambda)$ is essentially the normalized transmittance of the filter. The reason for the above modification is that when this constant is divided into the signal from the target, the result appears directly as spectral radiance.

The responsivity is represented by the slope of the curve on a graph of signal voltage (or other observable) out as a function of changes in the spectral radiance measured by the radiometer. The constancy of the responsivity is preserved up to those values of radiance which cause non-linear response in the detector. In this range the responsivity becomes a function of the input to the system, and care must be taken to consult the calibration curve and note carefully the responsivity for each signal out. It is best, if possible, to avoid the non-linear region (non-linear response sometimes signifies poor circuit design) and work only with constant responsivities. The non-linear region was never encountered in the present program.

Two independent methods were used for calibrating the NFOV radiometers, the collimator and distant extended source methods [4]. In the first, the aperture of a blackbody is placed at the focus of a collimator, fabricated in this case from optics identical to those used in the radiometers themselves. The radiometer is focussed for infinity and the signal output controlled by the radiance of the blackbody. The magnitude of the radiance was varied by changing the temperature of the blackbody. The measurements were made with each filter that was to be used in conjunction with a given radiometer in the field measurement. Curves on log-log paper of the preamplifier output voltage as a function of spectral radiance at the center wavelength of the filter are shown in figures 11 through 18. Table II lists the filter regions used with the different radiometers and the values L_λ/V_D and spectral responsivity of each determined from the curves drawn in the figures. Note that the responsivity values in table II are the values obtained for $\mathscr{R}_1'$ divided by $\Delta\lambda$.

The second method of radiance calibration, distant extended source, entails positioning the blackbody source far enough from the radiometer to obtain a good image of the aperture at the detector, and close enough to have the image appear larger than the detector. The spectral radiance values were varied again by changing the temperature of the blackbody. Signal outputs were plotted on the same graphs used for the collimator method. The curve was found to coincide with that plotted from the collimator method of calibration.

4.3.2. WIDE-FIELD-OF-VIEW RADIOMETERS. In calibrating the WFOV radiometers we are interested in obtaining not the radiance, but the spectral radiant intensity, $I_\lambda(\lambda)$. This is obtained from the experimental value of the spectral irradiance $E_\lambda(\lambda)$ and the distance D to the source. Thus, if we rearrange the original equation to obtain

$$E_\lambda(\lambda) = \frac{L_\lambda(\lambda)\cdot\alpha\cdot\tau_a(\lambda)}{D^2} = \frac{I_\lambda(\lambda)\cdot\tau_a(\lambda)}{D^2}$$

we can combine the constants $\mathscr{R}$ and A into $\mathscr{R}''$ to obtain

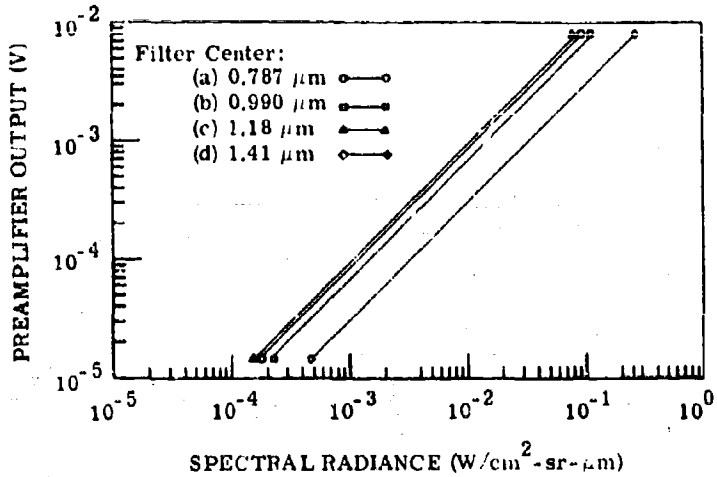

FIGURE 11. SIGNAL VOLTAGE vs. SPECTRAL RADIANCE WITH FOUR FILTERS FOR RADIOMETER #6

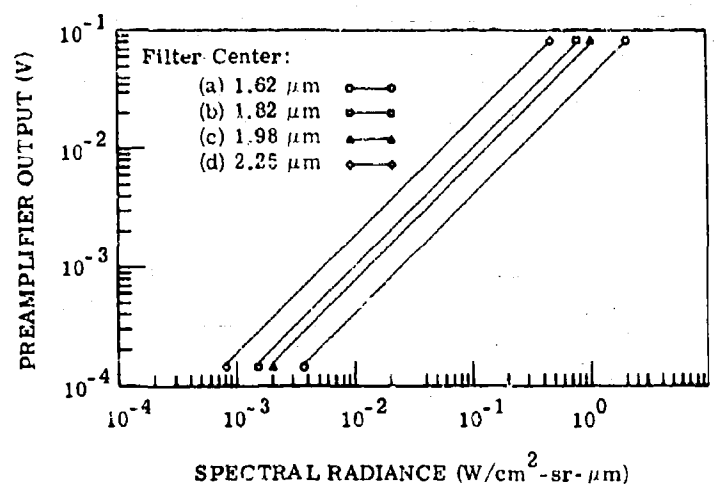

FIGURE 12. SIGNAL VOLTAGE vs. SPECTRAL RADIANCE WITH FOUR OTHER FILTERS FOR RADIOMETER #6

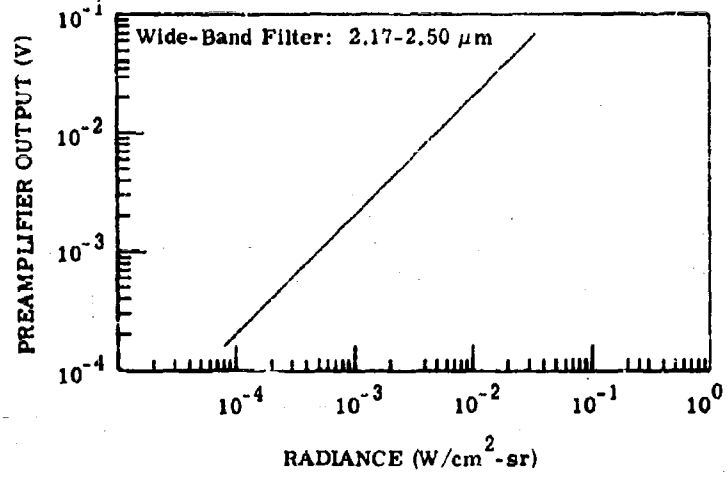

FIGURE 13. SIGNAL VOLTAGE vs. RADIANCE IN Δλ FOR RADIOMETER #6

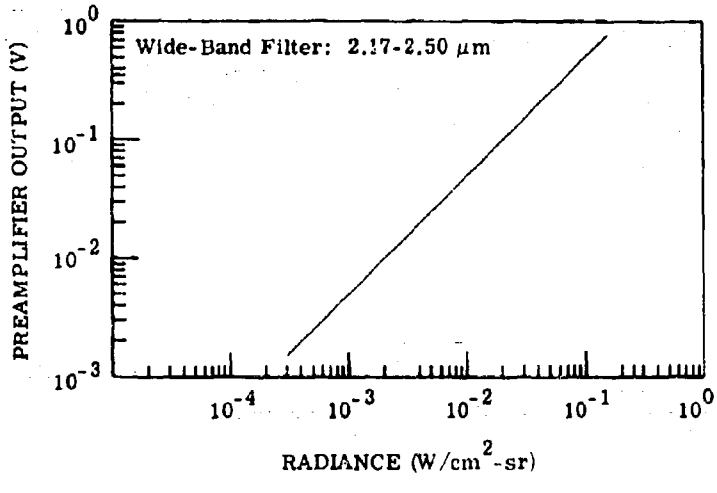

FIGURE 14. SIGNAL VOLTAGE vs. RADIANCE IN Δλ FOR RADIOMETER #7

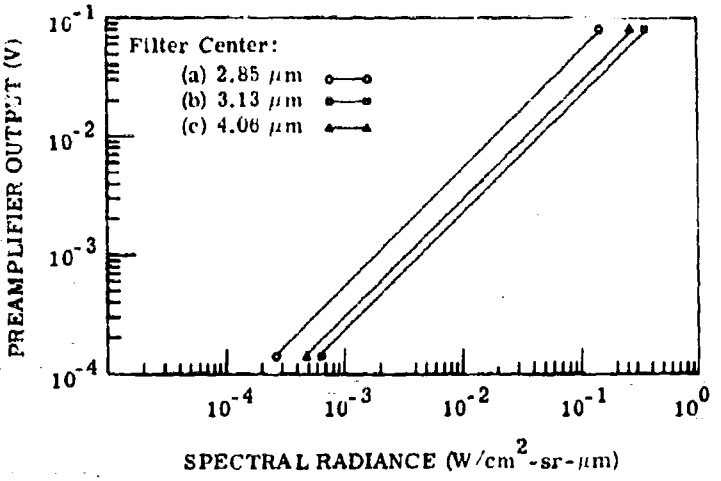

FIGURE 15. SIGNAL VOLTAGE vs. SPECTRAL RADIANCE WITH THREE FILTERS FOR RADIOMETER #7

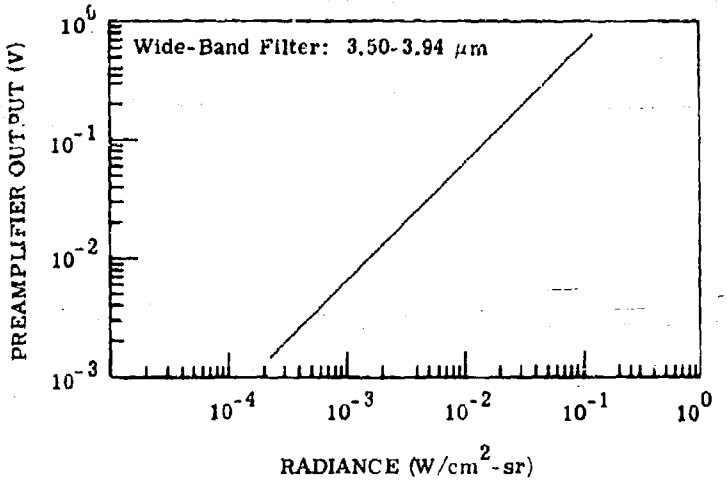

FIGURE 16. SIGNAL VOLTAGE vs. RADIANCE IN Δλ FOR RADIOMETER #7

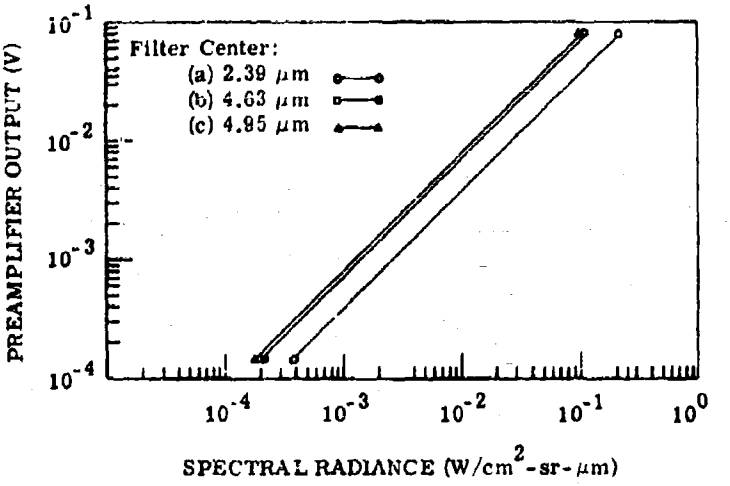

FIGURE 17. SIGNAL VOLTAGE vs. SPECTRAL RADIANCE WITH THREE FILTERS FOR RADIOMETER #8

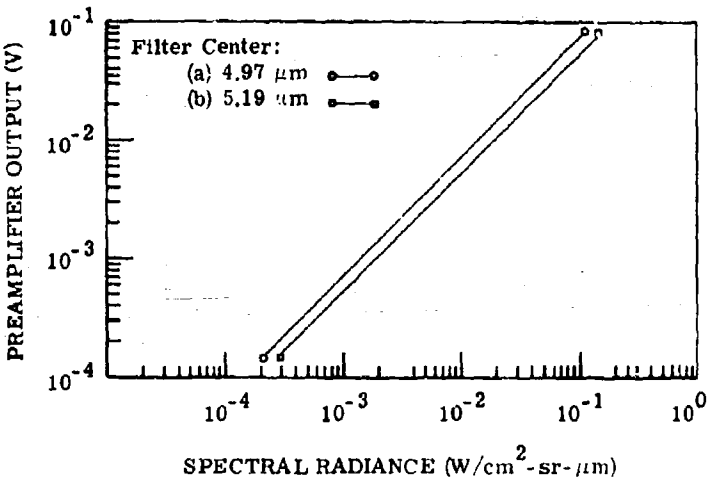

FIGURE 18. SIGNAL VOLTAGE vs. SPECTRAL RADIANCE WITH TWO FILTERS FOR RADIOMETER #8

TABLE II. RADIANCE RESPONSIVITIES FOR THE NFOV RADIOMETERS

Radiometer No.	Figure and Curve No.	Center λ (μm)	$L_\lambda/V_D\left(=\frac{1}{\mathscr{R}''_1}\right)$ (W-cm^{-2}-sr^{-1}-μm^{-1}/V)	Radiance Responsivity ($\mathscr{R}''$) (V/W-cm^{-2}-sr^{-1})
6	11 (a)	0.787	11.6	0.95
6	11 (b)	0.990	14.3	0.73
6	11 (c)	1.18	10.6	1.89
6	11 (d)	1.41	32.2	0.23
6	12 (a)	1.62	25.0	0.60
6	12 (b)	1.82	10.3	1.28
6	12 (c)	1.98	13.4	0.80
6	12 (d)	2.25	5.55	1.46
6	13	2.17-2.50 wide	0.475*	
7	14	2.17-2.50 wide	0.202*	
7	15 (a)	2.85	1.75	
7	15 (b)	3.13	4.20	3.72
7	15 (c)	4.06	3.30	3.92
7	16	3.50-3.94 wide	0.154*	
8	17 (a)	2.39	2.65	3.77
8	17 (b)	4.63	1.40	7.93
8	17 (c)	4.93	1.27	8.36
8	18 (a)	4.97	1.36	10.08
8	18 (b)	5.19	1.85	6.21

*These values are for the total bandwidth of the filter.

$$V = \mathscr{R}'' \int_{\lambda_1}^{\lambda_2} E_\lambda(\lambda) s(\lambda)\, d\lambda$$

when the region of integration is restricted to the spectral region of sensible transmission of the filter. Strictly speaking, $I_\lambda(\lambda) = \int_\alpha L_\lambda(\lambda)\, d\alpha$; not $I_\lambda(\lambda) = L_\lambda(\lambda)\cdot\alpha$. From this we get

$$\mathscr{R}'' = \frac{V}{\int_{\lambda_1}^{\lambda_2} E_{\lambda,BB}(\lambda) s(\lambda)\, d\lambda}$$

when we calibrate with a suitable blackbody source. If, as for the radiance calibration, we wish to obtain the spectral irradiance (i.e., $W/cm^2\text{-}\mu m$) directly from the signal voltage resulting from target radiation, we must normalize the result of integration and obtain

$$\mathscr{R}_1'' = \frac{V}{\frac{1}{\Delta\lambda}\int_{\lambda_1}^{\lambda_2} E_{\lambda,BB}(\lambda)s(\lambda)\,d\lambda}$$

where

$$\Delta\lambda = \int_{\lambda_1}^{\lambda_2} s(\lambda)\,d\lambda$$

The value for $1/\mathscr{R}_1'' = E_\lambda/V_D$ is given for each calibration in table III. Along with this quantity, table III also contains the irradiance responsivity $\mathscr{R}''$ for each calibration and the center wavelength of the filter used in each case.

The calibration is carried out in the laboratory by placing a blackbody at a focusable distance from the WFOV radiometer. The aperture of the blackbody is small enough to produce an image on the detector which is considerably smaller than the detector. The large range of irradiances used for calibrating the radiometers was obtained by varying the size of the blackbody aperture, the temperature of the blackbody, or the distance between the blackbody and the radiometer.

For each filter-radiometer combination the preamplifier output voltage caused by radiation from the blackbody was plotted on log-log paper as a function of the calculated spectral irradiance. These curves are presented in figures 19 through 26 for radiometers 1, 2, 3, and 4. The values for $E_\lambda/V_D = 1/\mathscr{R}_1''$ and for $\mathscr{R}''$, the spectral irradiance responsivity shown in table III, are obtainable from the curves. Note that the responsivity curves include an entry referring to a filter at 4.14 μm. In all other cases the filter regions used for the NFOV and WFOV radiometers were identical. In this case the filter for the NFOV radiometer complementary to the 4.14-μm filter was the one at 4.06 μm. They were intended to be identical, but a measurement of the spectral transmittance showed that they were slightly different.

4.4. CALIBRATION LAMPS

As part of the calibration procedure, it is necessary to determine if there are changes in the responsivity from one run to the next. This is done by fabricating simple lamps which have a constant, though not necessarily known, output. These lamps are clamped to the radiometer and the output observed.

TABLE III. IRRADIANCE RESPONSIVITIES FOR THE WFOV RADIOMETERS

Radiometer No.	Figure and Curve No.	Center λ (μm)	$E_\lambda/V_D\left(=\frac{1}{\mathscr{R}''_1}\right)$ (W-cm^2-μm/V)	Irradiance Responsivity ($=\mathscr{R}'$) (V/W-cm^2)
1	19 (a)	0.787	4.10×10^{-3}	2.68×10^{3}
1	19 (b)	0.990	3.72×10^{-3}	2.66×10^{3}
1	19 (c)	1.18	2.60×10^{-3}	7.70×10^{3}
1	20 (a)	1.41	6.90×10^{-3}	1.09×10^{3}
1	20 (b)	1.62	3.60×10^{-3}	4.15×10^{3}
1	20 (c)	2.85	1.06×10^{-3}	8.90×10^{3}
2	21 (a)	4.63	1.02×10^{-4}	10.90×10^{4}
2	21 (b)	4.93	9.50×10^{-5}	11.20×10^{4}
2	21 (c)	4.97	1.58×10^{-4}	8.66×10^{4}
2	21 (d)	5.19	2.05×10^{-4}	5.61×10^{4}
3	22 (a)	2.85	8.50×10^{-4}	1.10×10^{4}
3	22 (b)	3.13	5.80×10^{-4}	2.69×10^{4}
3	22 (c)	4.14	2.93×10^{-4}	4.88×10^{4}
3	22 (d)	4.63	1.20×10^{-4}	9.25×10^{4}
3	23	3.50-3.94 wide	7.70×10^{-6}*	
3	24 (a)	4.93	1.20×10^{-4}	8.86×10^{4}
3	24 (b)	4.97	1.44×10^{-4}	9.51×10^{4}
3	24 (c)	5.19	2.08×10^{-4}	5.52×10^{4}
4	25 (a)	1.82	1.36×10^{-3}	9.67×10^{3}
4	25 (b)	1.98	1.03×10^{-3}	1.04×10^{4}
4	25 (c)	2.25	4.15×10^{-4}	1.96×10^{4}
4	25 (d)	2.39	4.70×10^{-4}	2.12×10^{4}
4	26	2.17-2.50 wide	7.10×10^{-5}*	

*These values are for the total bandwidth of the filter.

The lamp used in checking the stability of radiometer responsivity was the General Electric Miniature Quartzline incandescent lamp #1973. The filament leads extend through the base of the lamp and for the current application were mounted inside a metal box to posts which were wired to a well-regulated source of 1.5 A dc. The lamp is rated at 12 W, but in this application it was operated at 7 W. It was sufficiently aged so that during the period of use there was no significant change in the radiant output.

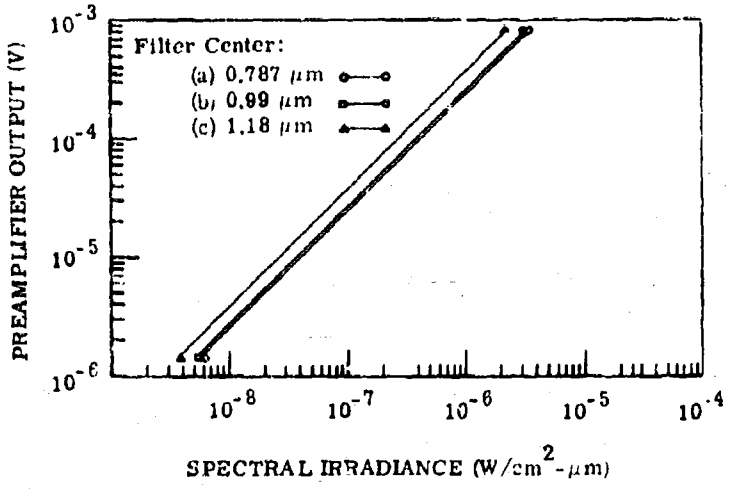

FIGURE 19. SIGNAL VOLTAGE vs. SPECTRAL IRRADIANCE WITH THREE FILTERS FOR RADIOMETER #1

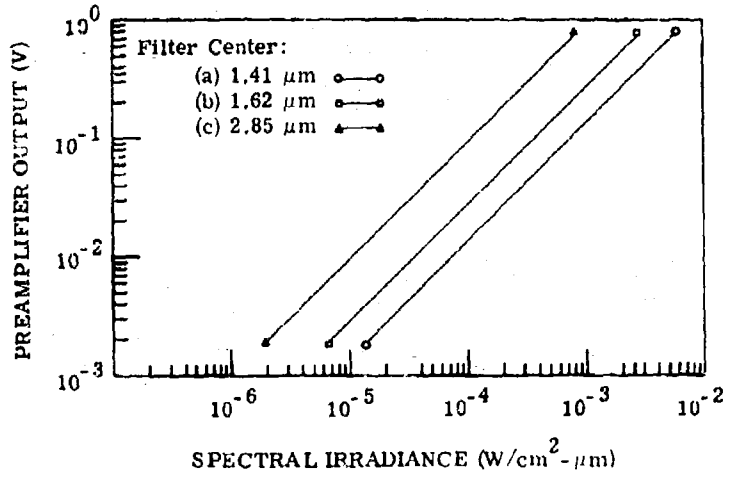

FIGURE 20. SIGNAL VOLTAGE vs. SPECTRAL IRRADIANCE WITH THREE FILTERS FOR RADIOMETER #1

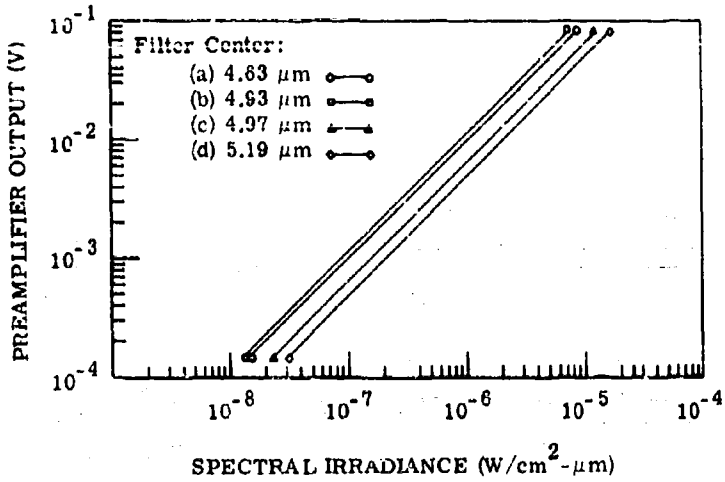

FIGURE 21. SIGNAL VOLTAGE vs. SPECTRAL IRRADIANCE WITH FOUR FILTERS FOR RADIOMETER #2

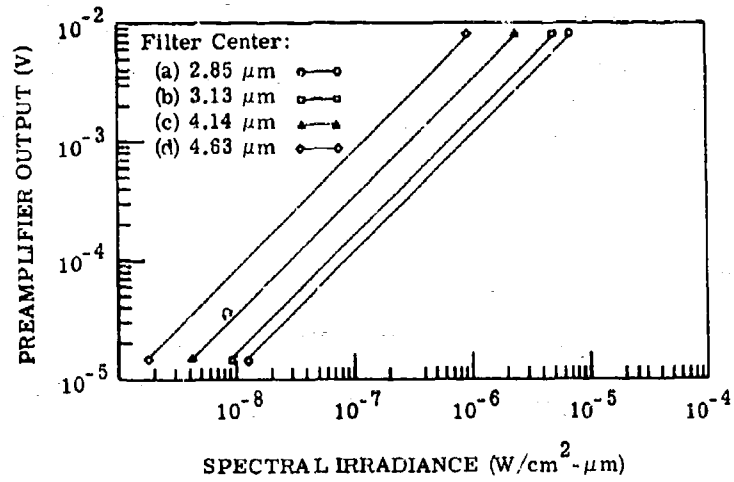

FIGURE 22. SIGNAL VOLTAGE vs. SPECTRAL IRRADIANCE WITH FOUR FILTERS FOR RADIOMETER #3

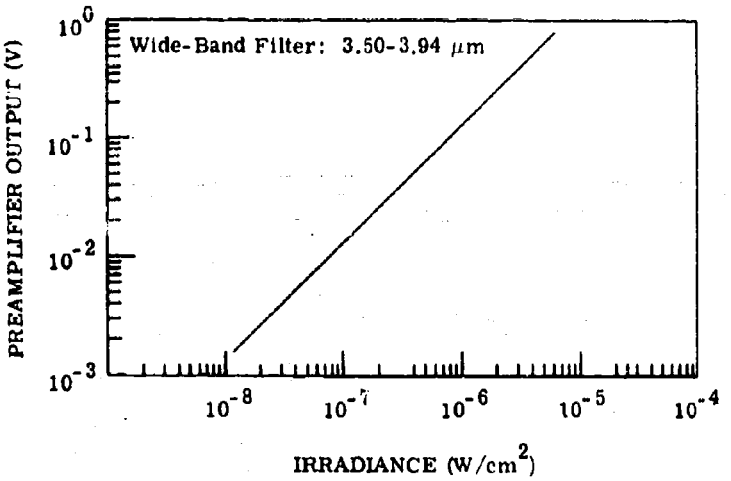

FIGURE 23. SIGNAL VOLTAGE vs. IRRADIANCE IN Δλ FOR RADIOMETER #3

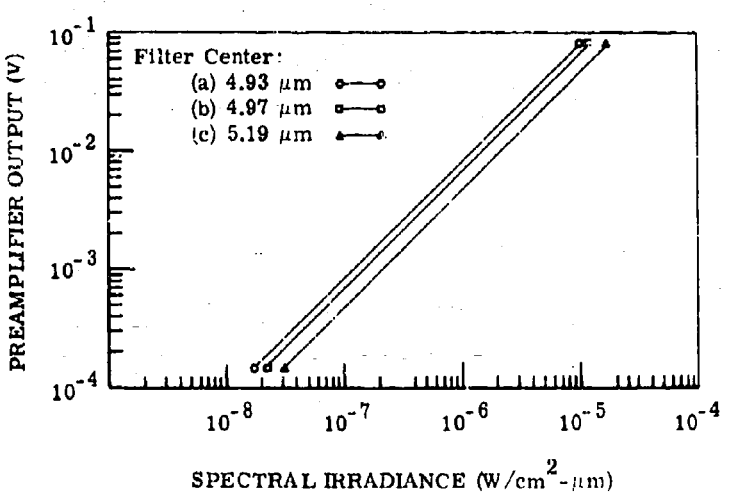

FIGURE 24. SIGNAL VOLTAGE vs. SPECTRAL IRRADIANCE WITH THREE FILTERS FOR RADIOMETER #3

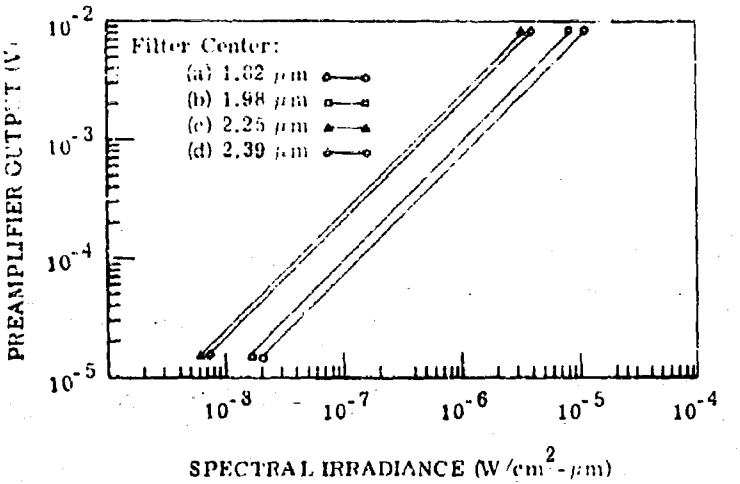

FIGURE 25. SIGNAL VOLTAGE vs. SPECTRAL IRRADIANCE WITH FOUR FILTERS FOR RADIOMETER #4

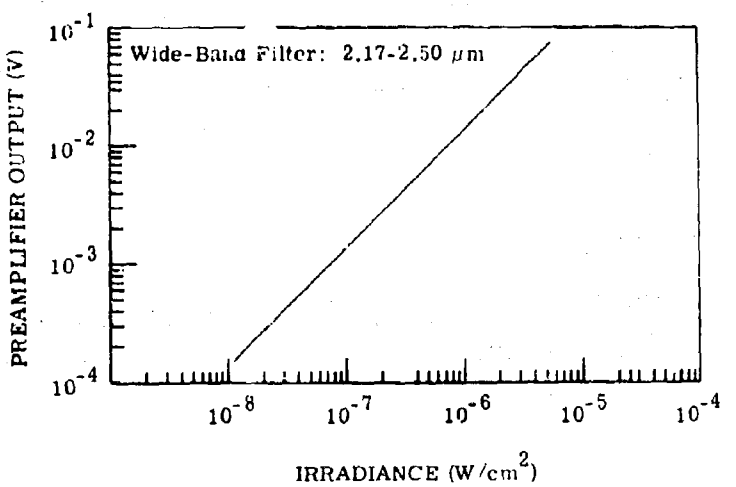

FIGURE 26. SIGNAL VOLTAGE vs. IRRADIANCE IN Δλ FOR RADIOMETER #4

Radiation from the lamp was observed through a small hole in a baffle plate covering the metal box. A small chopper was installed inside the box just in front of the lamp to provide a chopped signal source for the ac-coupled radiometers. For the WFOV radiometers the lamp housing was fitted directly to the snout of the radiometer. The radiation was observed through the 2.85-μm filter for radiometer #1, the 4.63-μm filter for radiometer #2, the 4.14-μm filter for radiometer #3, and the 2.59-μm filter for radiometer #4.

On the NFOV radiometers the lamp was mounted to the front in such a way that the hole in the baffle plate was lined up with the clear portion of the entrance mirror between the spider posts holding the secondary mirror in place. Because of the low signal levels, no filter was used in checking the NFOV radiometers.

4.5. ATMOSPHERIC TRANSMITTANCE

As an additional part of the calibration procedure, it is essential to determine the effect of the atmosphere on the propagation of radiation in the different spectral regions. Recall from section 4.3 that for the NFOV radiometer

$$V = \mathscr{R}' \int_{\Delta\lambda} L_\lambda(\lambda)\,\tau_a(\lambda)s(\lambda)\,d\lambda$$

and for the WFOV radiometer

$$V = \mathscr{R}'' \int_{\Delta\lambda} \frac{I_\lambda(\lambda)}{D^2}\,\tau_a(\lambda)s(\lambda)\,d\lambda$$

Therefore, in contrast to the measurements made in calibration where the absorption by atmospheric constituents was negligible, the signals from the target flashes inherently contained the atmospheric transmittance, $\tau_a(\lambda)$. Although removal of the effect of absorption is not necessarily (and not usually) a simple matter, for the narrow bandwidths used in this experiment it is believed that the spectral nature of the source did not vary radically within these bandwidths; thus there is no great error introduced by calculating as follows

$$L_\lambda(\lambda) = \left(\frac{1}{\tau_a}\right)\frac{V_{NFOV}}{\mathscr{R}_1'} \tag{1}$$

or

$$I_\lambda(\lambda) = \left(\frac{1}{\tau_a}\right)\frac{V_{WFOV}}{\mathscr{R}_1''}\,D^2 \tag{2}$$

where V_{NFOV} preamplifier output voltage for the NFOV radiometer

V_{WFOV} preamplifier output voltage for the WFOV radiometer

$$\bar{\tau}_a \quad \int_{\Delta\lambda} \tau_a(\lambda)s(\lambda)X(\lambda)\,d\lambda \Big/ \int_{\Delta\lambda} s(\lambda)X(\lambda)\,d\lambda$$

$X(\lambda)$ is a function designed to approximate the spectral distribution of the target, a 1000°K blackbody function in this case

If the target spectrum varies greatly from $X(\lambda)$, then large errors can be incurred depending on how the target and atmosphere interact spectrally. The value of $\bar{\tau}_a$ can be obtained in several ways. The two most direct approaches are (1) to measure spectrally, i.e., $\tau_a(\lambda)$, the transmittance of the atmosphere between the target and receiver using a blackbody as the known source of radiation, and calculate $\bar{\tau}_a$ from the above equation, and (2) to determine the amount of absorber in the path (e.g., by a relative humidity measurement in the case of H_2O vapor) and calculate $\tau_a(\lambda)$ from an appropriate model for this path, then calculate $\bar{\tau}_a$ as in the first method.

The first method is more accurate because $\tau_a(\lambda)$ is measured directly instead of calculated. However, it is more difficult and time consuming to implement. Furthermore, for the distances involved, the inaccuracy is probably no greater than that introduced by the variability of the data from the target flashes or the uncertainty in the interaction of the variable target spectrum and variable atmospheric absorption. Therefore, the second method was chosen for the determination of $\bar{\tau}_a$.

4.6. TEMPORAL RESPONSE

From previous experience it was known that the events to be measured had durations from a few milliseconds to several hundredths of a second and rise times as small as a fraction of a millisecond. These factors required that the radiometers be capable of holding a dc level for as long as a tenth of a second and have rise times of some tens of microseconds in order to accurately portray the shape of the observed pulse. This corresponds to a bandwidth of about 2 Hz to 17 kHz. Thus, relatively fast detectors were required which cover the spectral region 0.8 to 5 μm. Photovoltaic InSb and InAs detectors mounted in simple liquid nitrogen Dewars were the most timely and economical choices. Both of these detector types have intrinsic time constants of the order of a microsecond, but the time constant of the complete radiometer is determined by the coupling of the detector and its associated capacitance to the preamplifier. These detectors have relatively large impedances and when irradiated act like photocurrent generators. For best detectivity, this photocurrent should be measured with zero voltage drop across the detector. This condition can be met in several ways.

The first is by using a transformer to couple the detector to the preamplifier. In this way the dc voltage across the detector is kept low and the ac signal is amplified. Transformer coupling poses a problem in satisfying the low frequency requirement needed for this program. Frequencies lower than about 10 Hz can be difficult to transfer in a transformer. Hum pickup and non-linearity can also be problems. This solution was, therefore, rejected.

The second method is back-biasing the detector to obtain the required zero dc voltage drop and amplifying the small ac voltage in a low-noise voltage preamplifier. This solution is useful provided high frequency response can be traded for detectivity, since the detector capacitance combines with the preamplifier input impedance to determine the time constant of the combination. In our program, because of the large detectors involved (and hence large capacitances), this approach would have resulted in an unacceptably large loss of detectivity for the bandwidth required.

The third technique is to use an operational amplifier* as a current-to-voltage transducer. This technique transforms the photocurrent output to a voltage developed across a low output impedance and at the same time maintains an essentially zero voltage drop across the detector. No bandwidth sacrifices are required with this technique provided the operational amplifier has sufficient bandwidth. On the advice of a manufacturer's representative we tried the Fairchild μA709 silicon monolithic operational amplifier connected as a current-to-voltage transducer and had excellent results. This device is readily available, inexpensive, and has a low noise level.

The devices so constructed had equivalent input noise levels approximating the noise level of the InSb detectors, but about a factor of 5 to 10 above the noise level of the InAs detectors. Other techniques were tried in order to obtain a system with a noise level of the order of that of the InAs detectors, still maintaining the required bandwidth, but without success. We decided to accept the factor of 5 to 10 loss in detectivity on the InAs detectors in order to preserve the required bandwidth. A schematic of the preamplifier used on the InSb and InAs detectors is shown in figure 27. The second operational amplifier serves as a voltage follower to drive the 500 ft of cable between the preamplifier and the postamplifiers and recorder. All resistors used were precision metal film resistors so that the gain would remain constant to less than 1% over the range of temperatures to be encountered in the field program.

*An operational amplifier is a wideband amplifier having, ideally, infinite gain and input impedance, and zero output impedance. A variety of analog operations can be performed on electrical signals with such a device by using various types and amounts of feedback and interconnecting them in various ways. Reference 5 gives a complete treatment of the uses of these operational amplifiers.

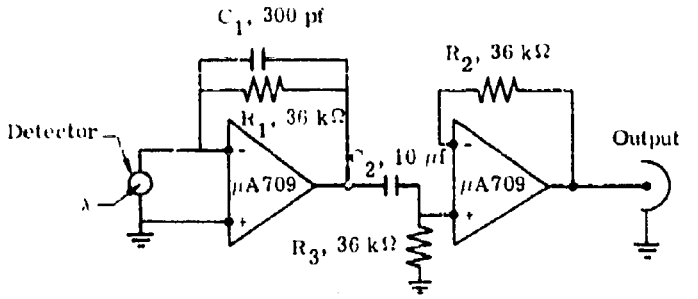

FIGURE 27. DIAGRAM OF DETECTOR PREAMPLIFIER. C_1 determines the high frequency cut-off of the radiometer, and C_2 the low frequency cut-off; for simplicity, battery power connections and phase-compensation components required in the operation of the μA709 have not been shown.

Subsequent to the field program, an investigation was made of the equivalent voltage and current input noise levels of the μA709 operational amplifiers that were used. At the same time similar tests were made on several other types of operational amplifiers available to us. These additional units were all epoxy-encapsulated units made up of discrete components. We came to the conclusion that for the detector sizes (2.5-mm square) and impedance values (15 kΩ to 80 kΩ) involved, the μA709 is the logical choice for all but the lowest noise level applications. To avoid completely limitations from amplifier noise, it would be necessary to use the most sophisticated of the hybrid high performance operational amplifiers now available.

It also became apparent during the course of testing some other detectors that if the size of the detector is smaller, so that the detector impedance is greater, the μA709 operational amplifiers become unsuitable because of their relatively moderate input impedance (~400 kΩ). In such cases it is necessary to go to high quality discrete component operational amplifiers with high impedance input circuitry.

During this post-field-program investigation, we also noted that the input noise voltages and currents of the 11 μA709 units tested varied between units by as much as a factor of 4. Thus, by careful selection it would have been possible to optimize the detectivity of the InAs radiometers more carefully. Table IV describes the detector used in each radiometer by radiometer number. The degree to which the detectivity of the radiometer approaches or exceeds the detector detectivity as measured by the manufacturer is an indication of the degree to which the preamplifier noise is smaller or greater than the detector noise.* It can be seen that in all

*It is not certain that all of the differences between detector and radiometer detectivities are due to the amplifier. The detectivity measurements made by the manufacturer were made at a different electrical frequency than those made by Willow Run Laboratories. Thus, some of the differences could be due to noise-spectrum differences at the two frequencies.

TABLE IV. RADIOMETER AND DETECTOR CHARACTERISTICS

Radiometer No.*	Detector Type and Serial No.	Detectivity of Detector (cm-Hz$^{1/2}$/W)**	Detectivity of Radiometer† (cm-Hz$^{1/2}$/W)	Detector Impedance (Ω)	Rise Time† (μsec)	Decay Time† (sec)
1	InAs, #0844	11.5×10^9	2.6×10^9	80 K	28	0.160
2	InSb, #0834	22.3×10^9	14.6×10^9	40 K	23	0.120
3	InSb, #0857	20.9×10^9	14.7×10^9	15 K	27	0.108
4	InAs, #0872	12.4×10^9	1.37×10^9	100 K	28	0.118
6	InAs, #0840	8.2×10^9	7.25×10^8	80 K	28	0.104
7	InSb, #0862	15.8×10^9	17×10^9		30	0.098
8	InSb, #0847	18.0×10^9	14.7×10^9	68 K	26	0.130
9	Hg:Cd:Te, #DLKB1	‡	‡	36	25	0.024

*The detector for radiometer 5 was irreparably broken in transit to Jefferson Proving Ground and is not included herein.

**As measured by detector manufacturer at 0 V bias.

†As measured by Willow Run Laboratories through the electronics used.

‡These characteristics are classified information.

cases but one* the radiometer detectivities were smaller than the corresponding detector detectivities. However, the loss of detectivity was significant only in the case of the InAs detectors.

One long-wavelength detector was also purchased for this program. It was a liquid-nitrogen-cooled Hg:Cd:Te photoconductive detector. These devices typically have very low resistances and very low responsivities, making it difficult to preserve their detectivities in real radiometers. This particular detector had a resistance of 34 Ω. In order to avoid a drastic loss in detectivity, it was necessary to use a transformer to couple the detector to the preamplifier. The preamplifier in this case was a simple voltage amplifier constructed of μA709 operational amplifiers. When so used its detectivity was satisfactory, but its bandwidth was somewhat below the desired level.

In the laboratory prior to the field program, some overshoot and ringing was also noted on this radiometer apparently due to the interaction of the transformer inductance and the blocking

*This occurrence of radiometer detectivity greater than detector detectivity is probably also indication of experimental differences between the manufacturer's measurements of detectivity and those of the Willow Run Laboratories.

capacitor required to keep the large dc bias current (necessary for a photoconductive detector) out of the transformer primary. At the time it was felt that this would not be a problem, and no further attempt was made to remove it prior to the field trip. However, during the field trip preliminary observations made with this radiometer showed high intensities dominated by this ringing. To eliminate this problem, the transformer was removed and the reduced detectivity accepted. However, at this time the detector developed a crack due to a defect in its window and lost its vacuum. It was returned to the manufacturer immediately for repair, but was not returned in time for the remainder of the field trip.

During the course of these tests the frequency response of each of the radiometers was measured using a gallium-arsenide-phosphide radiating diode driven by a very low-output impedance current booster, driven in turn by a square-wave generator. The radiating diode emits at 6900 Å with a radiant output rise time of about 10 nsec. We decided to observe the response of each radiometer to square-wave pulses rather than the amplitude response to continuous pure sine waves. The reason for this was that the events to be observed were to be pulses rather than continuous functions. Thus, observation of the pulse response of the radiometers would provide the most useful means of evaluating the temporal fidelity of the radiometer. Two parameters were measured from the pulse response. The rise time (the time for the output of the radiometer to go from 0.1 to 0.9 of its final level when the radiant input is a step function with very fast rise time) was measured which characterizes the high frequency response. The decay time (the time it takes for the radiometer to drop from 0.9 of its maximum value to 0.1 of its maximum value when the radiant input is a step function of essentially infinite length) was also measured to characterize the low frequency response. Figure 28 illustrates the quantities measured. Table IV also lists the rise times and decay times of the radiometers as used during the field program. All frequency response measurements were made by observing the signal as processed by the preamplifier, 500-ft cable, and postamplifier at the point where the signal entered the tape recorder. The square-wave pulse response of the tape recorder was observed separately and was within the manufacturer's specifications. Uniform response down to dc was evident and typical rise times of 15 μsec were measured although an overshoot of about 10% in a square-wave pulse was typically observed. The existence of the overshoot was not considered to be a serious drawback since it lasted for only about 15 μsec.

5
MEASUREMENT PROCEDURE

Measurements on this program were made at the Jefferson Proving Ground in Madison, Indiana, on essentially a non-interference basis. Although we had no control over the firing

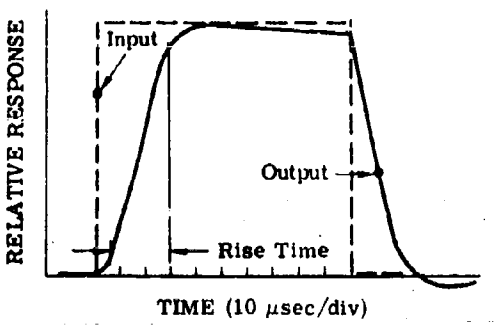

(a) Rise Time

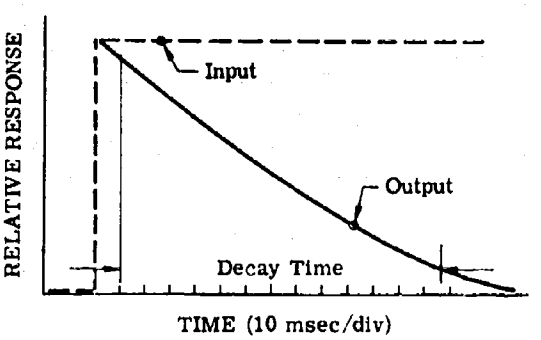

(b) Decay Time

FIGURE 28. DIAGRAM OF PULSE RESPONSE

schedule, we had the complete cooperation of the personnel there and were able to operate our equipment with relative freedom. Technically, the success of the program depended on our ability to get instrumentation in the field in as short a time as possible so that (1) we caused little interruptions to the firing schedule, and (2) we had more time to calibrate the instruments prior to the firing and to care for the details that help make an experiment successful. A very large factor in the success of an experiment of this type is the number of personnel available and the diligence with which they work to maintain peak performance. In this respect the crew for these experiments, both our own and the support staff from Jefferson Proving Ground, was unexcelled.

The instrumentation was carried in a government-furnished vehicle which was used both as a mobile laboratory installation and as a carrier for the equipment. The vehicle could be expanded for calibration and maintenance of instrumentation and retracted for transportation.

The retracted vehicle was driven to the firing range where the radiometric and recording gear were removed. The six radiometers were carried to a site roughly 200 to 400 ft from the gun position, depending on the expected intensity of muzzle flash. They were pointed at the front of the muzzle approximately perpendicular to the direction of fire (see figs. 29 and 30).

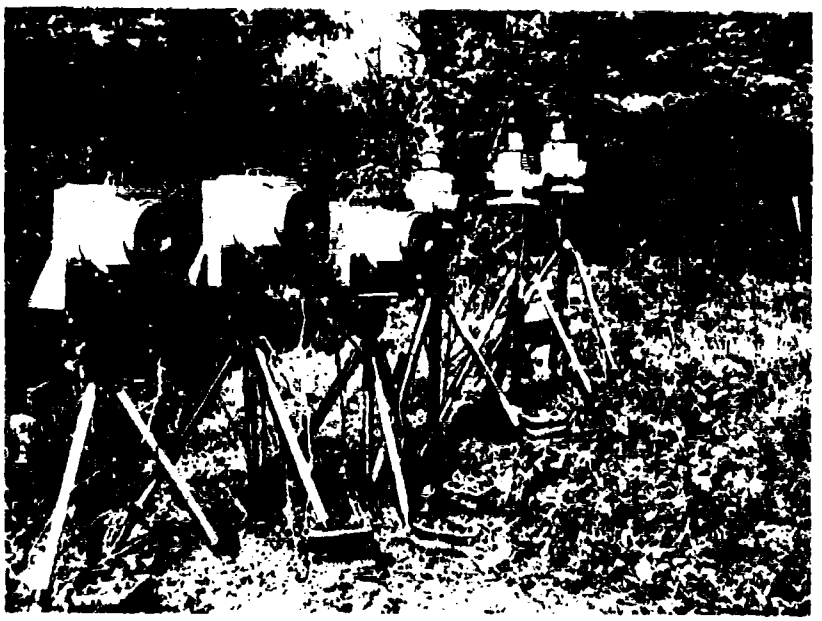

FIGURE 29. PHOTOGRAPH OF RADIOMETERS SET UP TO OBSERVE 81-mm MORTARS, 8/27/68. The narrow-field-of-view radiometers are on the left and the wide-field-of-view radiometers on the right.

The WFOV radiometers were aimed such that the total flash (including secondary burning) would be encompassed in the uniform portion of the measured field of view. The NFOV radiometers were aimed directly in front of the muzzle for observing the radiance of the plume. Figure 31 shows the relationship which was sought between the narrow field of view and the gun muzzle in aiming the NFOV radiometers. Because of the very small size of the field of view of these instruments, the repeatability of this aiming process was probably not good. Nevertheless, the consistency of the results obtained on different occasions indicated that the effects of these aiming difficulties was small. On several occasions a small chopped light source placed at the desired position was used as an aiming source. However, time limitations at Jefferson Proving Ground precluded the use of this source in most cases. The size of the portion of the plume observed was a direct function of the distance between the radiometers and the gun.

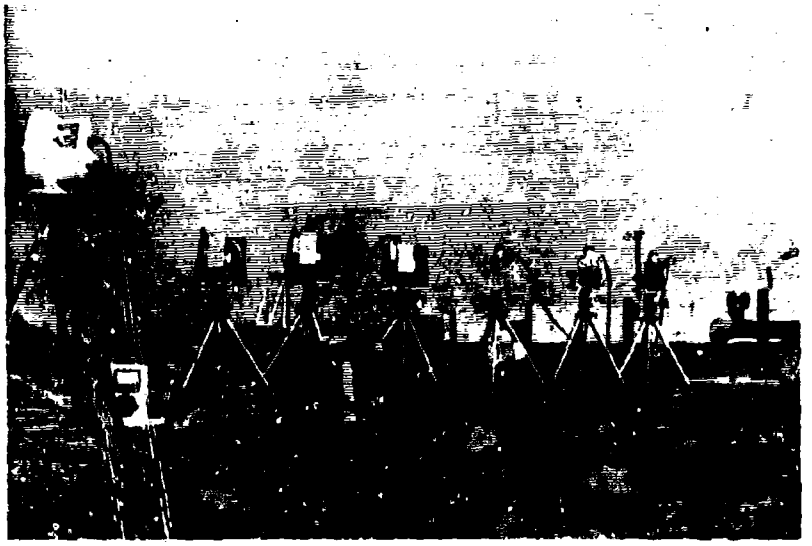

FIGURE 30. PHOTOGRAPHS OF RADIOMETERS SET UP TO OBSERVE THE 75-mm GUN. The Fastax camera is at the far left.

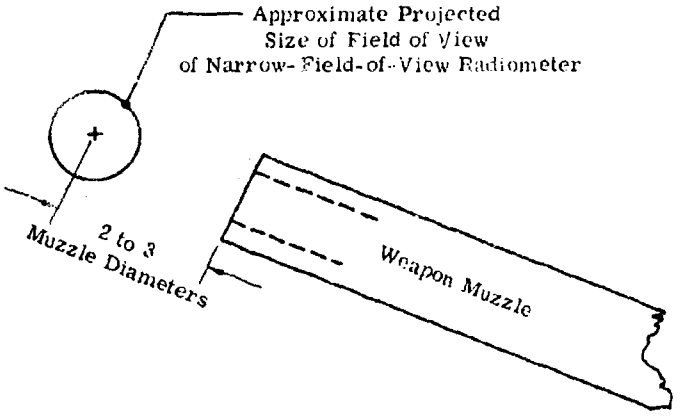

FIGURE 31. RELATIONSHIP BETWEEN FIELD OF VIEW OF THE NFOV RADIOMETERS AND THE GUN MUZZLE

The numbers and types of rounds fired were recorded.* Jefferson Proving Ground personnel recorded the relative humidity and temperature from which the atmospheric transmittance could be calculated. The filters were installed, and the detector Dewars were filled. Reels of cable were at the same time strung out for connections between the radiometers and the postamplifiers and recording equipment which were protected with the personnel behind an embankment some 200 to 500 ft distant. A Fastax camera supplied by the Army Missile Command was set up in the vicinity of the radiometers to obtain a time record of spatial changes of the plume observed in the visual region of the spectrum.

Radiometer signals corresponding to the muzzle flash were recorded on a 1-in. magnetic tape recorder, along with voice information identifying the rounds. At the same time any four of the six radiometers could be monitored in real time on oscilloscope traces (4 traces were available on 3 oscilloscopes). Such monitoring was used primarily as a guide for setting the gains on the postamplifiers as the rounds were fired. This insured that, at least for the later rounds of a series, the signal-to-noise ratio of each measurement was as high as practicable without encountering the saturation of the amplifier or tape recorder.

On almost every occasion a number of photographs of oscilloscope traces showing muzzle flash data in real time were obtained. These have not been presented in this report; rather, the traces included (see vol. II) were all obtained from a playback of the recorded data. However, the traces obtained in real time were compared with traces presented in volume II, and we established that the tape recorder did not distort the traces in any apparent way. A regulated square wave was recorded on all channels of each reel of tape for a duration of approximately 30 sec for calibration purposes.

After the rounds had been observed on each occasion, we had to remove all our equipment from the firing site and return it to our calibration site behind one of the office buildings. Altogether, on 15 days 1174 rounds were observed.

6
DATA REDUCTION

Upon return from the field trip and before analysis could be started, hard copies of the data had to be obtained to which the calibration data could be applied. After some experimentation with different oscilloscopes and cameras, we settled upon a standard 35-mm, single-lens

*The composition and characteristics of the powder in the individual firings are discussed in volume II of this report.

reflex camera equipped with an extension tube which was used to photograph oscilloscope traces of the data as the recorded results were played back. The 2-V, 1-kHz, square-wave signals recorded during the measurements on all channels of each tape were also played back and photographed. The amplitudes of all data traces were adjusted with the factor by which the appropriate square wave, as reproduced by the tape recorder, departed from 2 V. The gains as recorded during the field trip were applied to arrive at the preamplifier output voltage which would give one division deflection on the scope. Using the appropriate value from table II or III, either the spectral radiance or radiant intensity corresponding to one scope division was found using equation 1 or 2, whichever was appropriate.

In these equations, $\bar{\tau}_a$ was computed using an existing program [6] for computing spectral atmospheric transmittance $\tau_a(\lambda)$. The blackbody curve for 1000°K was assumed to crudely approximate the muzzle flash spectrum and so was used for $X(\lambda)$. Values of $\bar{\tau}_a$ were computed for each filter for 90 different paths on a digital computer. These paths corresponded to 5 path lengths from 75 to 300 ft, 5 ambient temperatures from 75 to 95°F, and 3 relative humidities, 50, 60, and 70%. The water-vapor path length in precipitable centimeters for each of these paths was also computed. To find the most appropriate value of $\bar{\tau}_a$ for a given measurement, the water-vapor path length corresponding to the ambient conditions was computed and a value for $\bar{\tau}_a$ chosen from the 90 values which most closely approximated the water vapor path length and physical path length of the measurement.

7
SUMMARY

The objective of this program was to obtain comprehensive data regarding the dynamic spectral emissions of various guns during firing. From a scientific point of view, however, we attempted to observe the radiation from as many guns and mortars as was feasible within constraints imposed by time, firing schedules, and experimental difficulties experienced in the field. Specifically, we were able to observe with varying degrees of success guns ranging in sizes from 40 to 175 mm and mortars from 60 mm to 4.2 in. (the 60-mm results were deleted from the program because the signal levels were too low).

To cover the range in spectrum we used a series of filters with the intent of obtaining data with approximately a 0.1-μm bandwidth at spectral intervals of approximately 0.2 μm in the region 0.7 to 5.3 μm. The original specification was to cover only this region, but we suggested that the region from 7.5 to 13.0 μm might be of equal importance, and it was agreed that we would include this region in the measurement program.

Whereas we are able to satisfy the broad objectives of the contract with the results reported in volume II, we are unable to satisfy fully the more stringent scientific goals set by ourselves in an attempt to produce as nearly complete a picture as possible of gun flash data. These goals are compromised by the following difficulties which were encountered in the course of the program:

(1) Financial constraints prohibited the use of duplicate filters to provide unambiguous, simultaneous measurement of spectral radiant intensity and spectral radiance in the same spectral region.

(2) In spite of the excellent rapport between us and the personnel at Jefferson Proving Ground, firing schedules were never totally consistent with our need for specific observations to provide a uniform density of data from the standpoints both of gun types and spectral region.

(3) Delivery schedules of component (specifically filter) suppliers were incompatible with our field program schedule, although delivery time was "guaranteed."

(4) Experimental hardships took the usual toll, particularly in time, but also unfortunately in data. Specifically, the loss of the long-wavelength detector because of a cracked window (due to stresses in manufacture) made it impossible to obtain any data in the long-wavelength region between 7.5 and 13.0 μm in the scheduled time of the field trip.

(5) A shortsighted estimate on our part of the enormous quantity of data we were actually able to obtain forced us to delete some of the many results we would like to have reported. To have included all of the useful data would have required an extension to the contract of both time and funding.

To assemble all the data required to give a complete picture of the radiative characteristics of gun flash, including the spectral region from 7.5 to 13 μm, would require another measurement program. To perform a more complete analysis of the data actually obtained, however, requires an extension to the analysis program incorporating the supporting data needed to yield an increased confidence in the radiation levels reported in volume II. It is recommended at this time that no further measurements be made, but that support be offered to perform the more complete analysis and to formulate predictive models for the radiative characteristics of gun flash.

REFERENCES

1. L. S. Herczeg, Investigation of the Spectral Emittance of Military Propellants (July to September 1952) (U), Report No. A-2258-1, The Franklin Institute, Laboratories for Research and Development, Philadelphia (CONFIDENTIAL) (AD 3490).

2. L. S. Herczeg, Investigation of the Spectral Emittance of Military Propellants (March to August 1954) (U), Report No. F-2258, The Franklin Institute, Laboratories for Research and Development, Philadelphia (CONFIDENTIAL) (AD 66009).

3. Spectral Characteristics of Muzzle Flash, AMC Pamphlet, The Franklin Institute, Laboratories for Research and Development, Philadelphia (AD 818 532).

4. F. E. Nicodemus and G. J. Zissis, Methods of Radiometric Calibration, Report No. 4613-20-R, Willow Run Laboratories, The University of Michigan, November 1956.

5. Applications Manual for Operational Amplifiers, Philbrick/Nexus Research, Dedham, Mass., 1968.

6. D. Anding, Band-Model Methods for Computing Atmospheric Slant-Path Molecular Absorption, Report No. 7142-21-T, Willow Run Laboratories of the Institute of Science and Technology, The University of Michigan, Ann Arbor, February 1967.

UNCLASSIFIED
Security Classification

DOCUMENT CONTROL DATA - R & D

(Security classification of title, body of abstract and indexing annotation must be entered when the overall report is classified)

1. ORIGINATING ACTIVITY (Corporate author)	2a. REPORT SECURITY CLASSIFICATION
Willow Run Laboratories of the Institute of Science and Technology, The University of Michigan, Ann Arbor	Unclassified
	2b. GROUP

3. REPORT TITLE

RADIOMETRIC MEASUREMENTS OF MUZZLE FLASH, Final Report, Volume I: Program Design and Procedure

4. DESCRIPTIVE NOTES *(Type of report and inclusive dates)*
Final Report

5. AUTHOR(S) *(First name, middle initial, last name)*
A. J. LaRocca, G. H. Lindquist, J. P. Livisay, C. J. Green

6. REPORT DATE	7a. TOTAL NO. OF PAGES	7b. NO. OF REFS
April 1969	viii + 40	6

8a. CONTRACT OR GRANT NO	9a. ORIGINATOR'S REPORT NUMBER(S)
DAAH01-68-C-1475 b. ARPA Order No. 859-7	1852-9-F(I)
c.	9b. OTHER REPORT NO(S) *(Any other numbers that may be assigned this report)*
d.	

10. DISTRIBUTION STATEMENT
This document is subject to special export controls and each transmittal to foreign governments or foreign nationals may be made only with prior approval of Assistant Chief of Staff for Intelligence, ATTN: ACSI-FE, Washington, D. C.

11. SUPPLEMENTARY NOTES	12. SPONSORING MILITARY ACTIVITY
	Advanced Research Projects Agency Department of Defense Washington, D. C.

13. ABSTRACT

Volume I begins with a description of the design of a program to measure the radiation from weapon muzzle flash in the spectral region from 0.8 to 5 μm. Instruments designed to measure the spectral radiant intensity and spectral radiance of these phenomena in narrow spectral bands are described. A discussion of the calibration techniques used to quantify accurately and precisely the results from the instruments is also included. The results of the measurements obtained are presented in Volume II.

DD FORM 1 NOV 68 1473

UNCLASSIFIED
Security Classification

14 KEY WORDS	LINK A		LINK B		LINK C	
	ROLE	WT	ROLE	WT	ROLE	WT
Radiometers						
Muzzle flash detection						
Weapons location						
Radiative characteristics						
Narrow-band filters						
Wide-band filters						
Detectors						